(A)

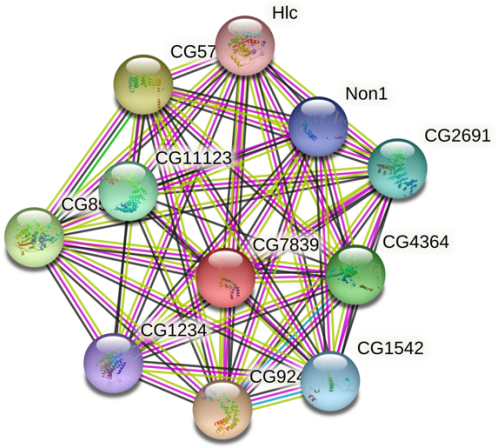

(B)

Your Input:

		Neighborhood	Gene Fusion	Cooccurence	Coexpression	Experiments	Databases	Textmining	[Homology]	Score
CG7839	IP14658p; Sequence-specific DNA binding transcription factor activity. It is involved in the biological process described with: regulation of transcription, DNA-templated; neurogenesis (1174 aa)									

Predicted Functional Partners:

CG9246	Nucleolar complex protein 2 homolog; It is involved in the biological process described with: neurogenesis				●	●		●		0.997
CG5728	LD41803p; mRNA binding. It is involved in the biological process described with: regulation of alternative mRNA splicing, via ...				●	●		●		0.995
CG8545	LD11307p; RNA binding; S-adenosylmethionine-dependent methyltransferase activity. It is involved in the biological process d...				●	●		○		0.995
CG4364	Pescadillo homolog; Required for maturation of ribosomal RNAs and formation of the large ribosomal subunit				●	●		●		0.988
CG11123	RH42110p; RNA binding				●	○		●		0.984
CG2691	RRP12-like protein; It is involved in the biological process described with: neuron projection morphogenesis				●	●		●		0.982
CG1542	Probable rRNA-processing protein EBP2 homolog; Required for the processing of the 27S pre-rRNA				●	●		●		0.982
Non1	Nucleolar GTP-binding protein 1; Involved in the biogenesis of the 60S ribosomal subunit (By similarity). Required for normal ...				●	●		●		0.982
CG1234	annotation not available				●	○		●		0.981
Hlc	Helicase, isoform A; ATP binding; ATP-dependent RNA helicase activity; nucleic acid binding. It is involved in the biological pr...				●	●		○		0.979

Fig. S1. Protein-protein interaction network generated using STRING (Szklarczyk et al., 2019)

(A) Graphic representation and (B) predicted list of the functional partners of NOC1/CG7839, members of the interaction network.

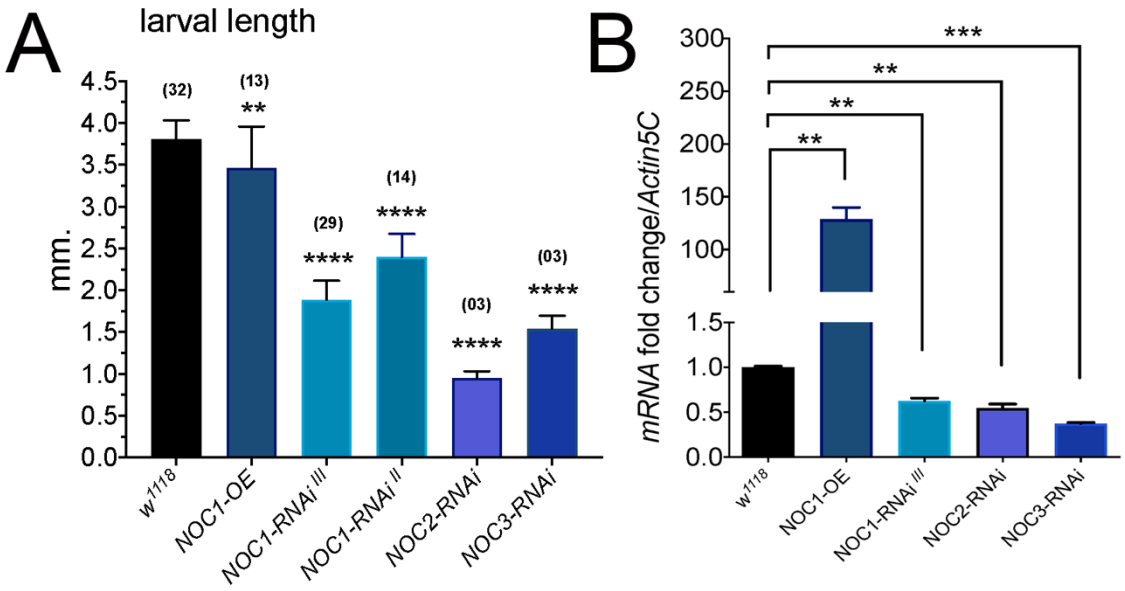

Fig. S2A-B. Length of larvae (A) and the relative mRNA expression (B) in whole larvae overexpressing *NOC1* or with downregulation of *NOC1, 2* and *3* using the *actin-Gal4* promoter.

(A) Larval Length was measured at 120 hours AEL. The asterisks represent the *p*-values from one-way analysis of variance (ANOVA) with Tukey multiple comparisons ** = $p < 0.01$ and **** = $p < 0.0001$, and the error bars indicate the standard deviations for each genotype. In parenthesis is indicated the number of animals analyzed. (B) qRT-PCR showing the relative amount of *NOCs mRNA* upon RNA overexpression or interference. *NOC1-OE* and *NOCs-RNAi* were ubiquitously expressed using the *actin-Gal4* promoter. RNA was extracted from whole larvae. *p*-values were calculated from Student's *t*-test from at least two independent experiments: ** = $p < 0.01$, *** = $p < 0.001$ and **** = $p < 0.0001$, the error bars indicate the standard deviations.

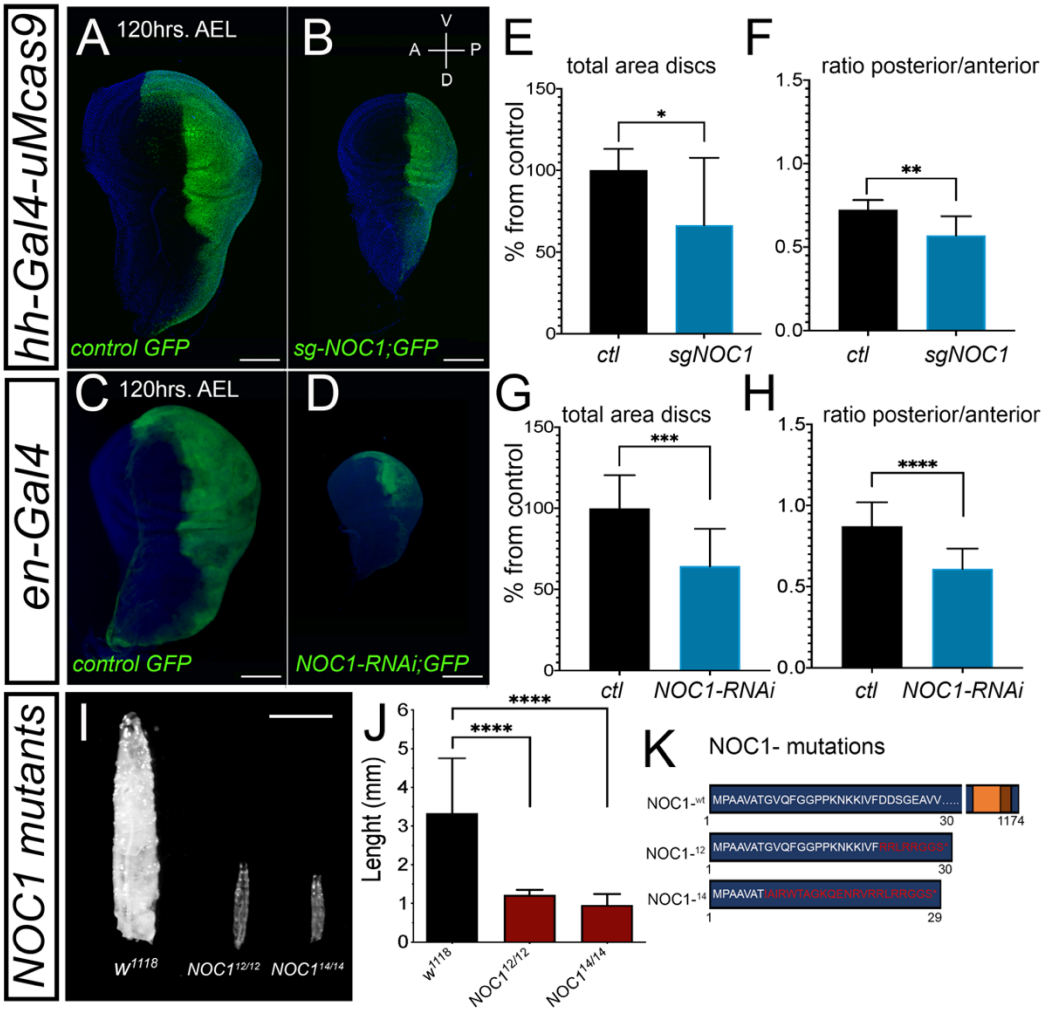

Fig. S3. NOC1 CRISPR mutation affects animal growth and phenocopies NOC1 downregulation induced by RNA interference in the wing disc.

To develop genomic *NOC1* mutants, we induced site specific mutations with the CRISPR-Cas9 system, using the line *sgRNA*^{CG7839} from Boutros's laboratory (Port et al., 2020). To analyze if the reduction of NOC1 with this system phenocopied the data with *engrailed*-Gal4, we used a line that carries the *hedgehog-Gal4* to drive *UAS-Cas9* to express *sgRNA*^{CG7839} in the posterior compartment of the wing disc. As shown in Figure A-B, driving mutations of NOC1 using *hedgehog-Gal4* compromised and reduced the development of the posterior compartment of the wing disc within a similar extent to that observed with *engrailed-NOC1-RNAi* (C-D). To compare the efficiency of the two systems, we analyzed the total area of imaginal discs and the ratio between the area of the posterior compartment (marked by co-expression of GFP) and the anterior from animals at 120 hours AEL. This analysis showed that reduction of NOC1 using *sgRNA*^{CG7839} affected the total area of the discs and the ratio between the posterior and the anterior compartments (E-F). These data resembled that obtained using NOC1-RNAi expressed under the *engrailed* promoter (G-H). To introduce NOC1 mutations in the germ line, we used the *nos-Gal4, UAS-Cas9* line crossed with *sgRNA*^{CG7839}. Sequencing analysis of 30 NOC1 heterozygous lines revealed the presence of missense mutations in the NOC1 gene in two lines, which encoded for very short polypeptides of 30 and 29 amino acids in length in *NOC1-mut12* and *NOC1-mut14*, respectively (K). Moreover, the phenotypic analysis of these two homozygous NOC1 mutants showed a robust growth defect at the larval stage (I and J, also shown in Figure 1C), recapitulating the phenotype described in the *actin-NOC1-RNAi* larvae (Figure 1B).

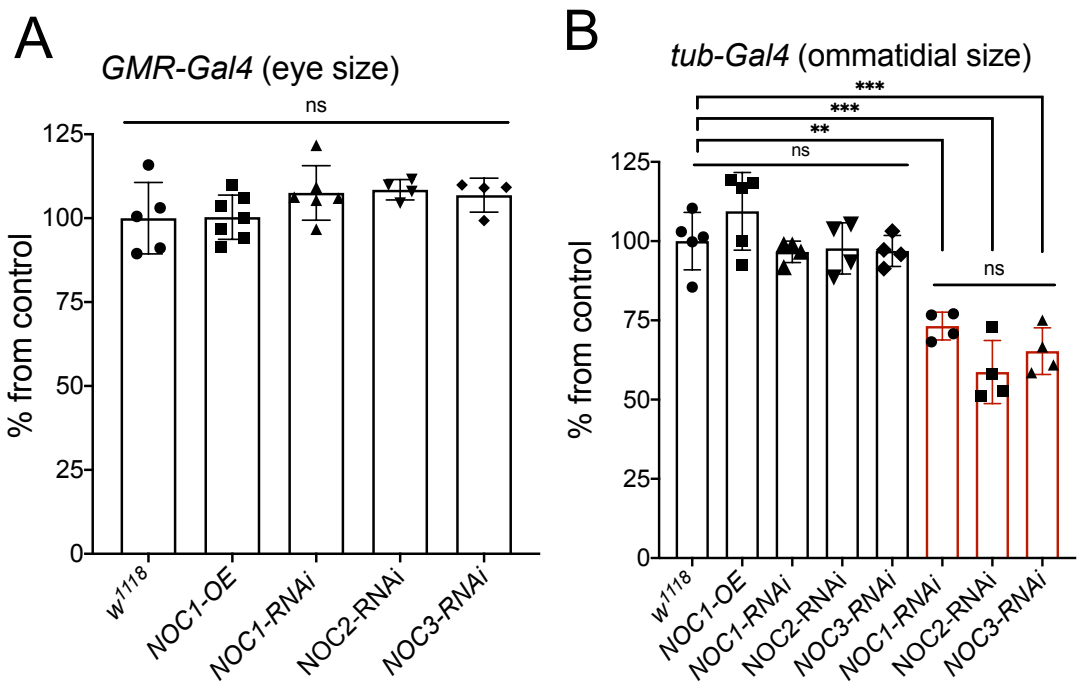

Fig. S4. (A) Quantification of the eye size from animals expressing the indicated transgenes using the *GMR-Gal4* promoter, (B) or the ommatidial size using the *tubulin-Gal4* promoter. Values are expressed as % from the control. Statistical analysis was calculated using Student's *t*-test from the number of animals indicated in the experiment. The error bars indicate the standard deviations.

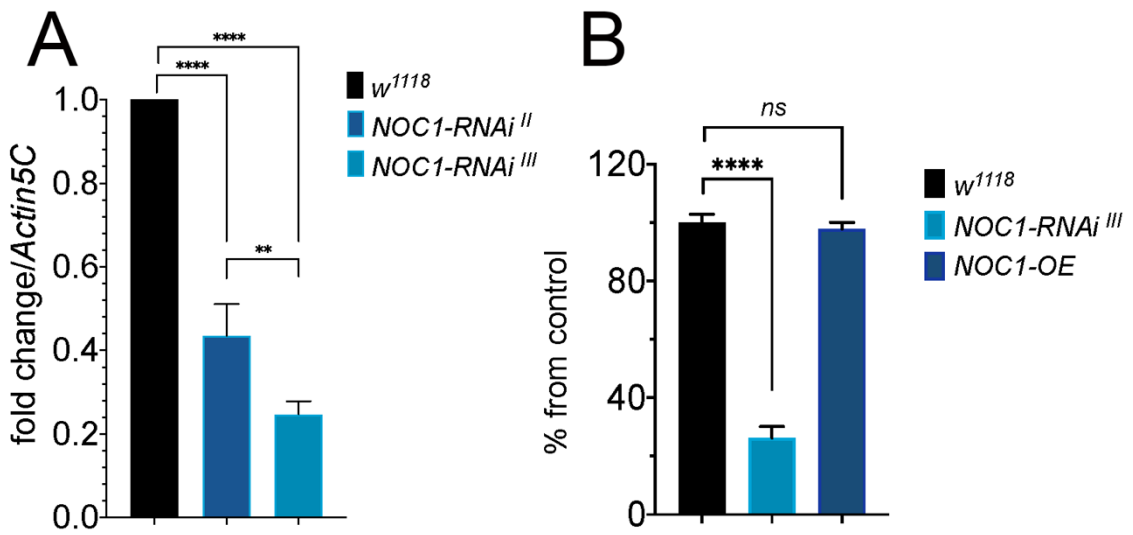

Fig. S5 A-B. (A) qRT-PCR showing the relative amount of *NOC1 mRNA* upon expression of the indicated transgenes using the ubiquitous *actin-Gal4* promoter. RNA was extracted from whole larvae. *p*-values were calculated from Student's *t*-test from at least two independent experiments: ** = $p < 0.01$, **** = $p < 0.0001$, the error bars indicate the standard deviations. **(B) Analysis of the size of wings in adult females of the indicated genotypes.** *p*-values were calculated from Student's *t*-test from at least two independent experiments: * = $p < 0.05$, ** = $p < 0.01$, **** = $p < 0.0001$, the error bars indicate the standard deviations. At least 10 animals were used for w^{1118} and *NOC1-OE*, while for *NOC1-RNAi*$^{-II}$ only 4 were born as adults (escapers).

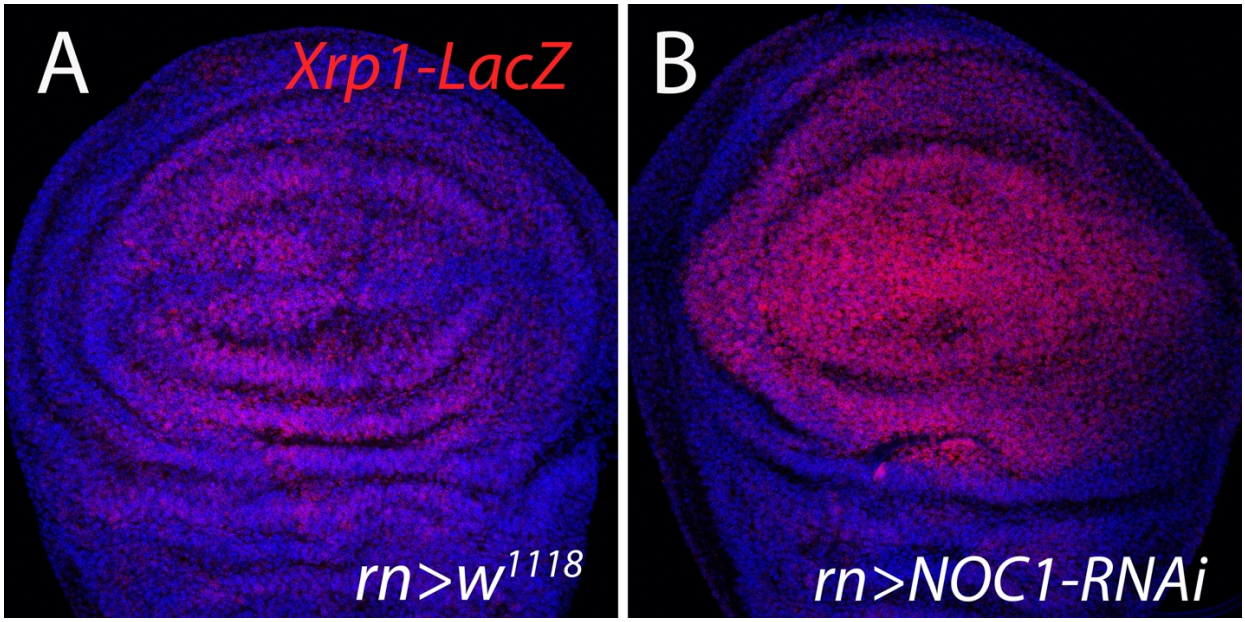

Fig. S6. Confocal images of wing imaginal discs showing increased activation of Xrp1 promoter upon expression of NOC1-RNAi using the *rotund-Gal4* promoter. *NOC1-RNAi* was expressed using the *rn-Gal4* promoter in a line carrying the $Xrp1^{02515}$-lacZ as a reporter for the activation of XRP1 (Baillon et al., 2018). Third instar imaginal discs were dissected and analyzed for LacZ expression using anti-beta gal antibody (red). Nuclei were stained with Hoechst (blue). $w^{1118}Xrp1^{02515}$ was used as control.

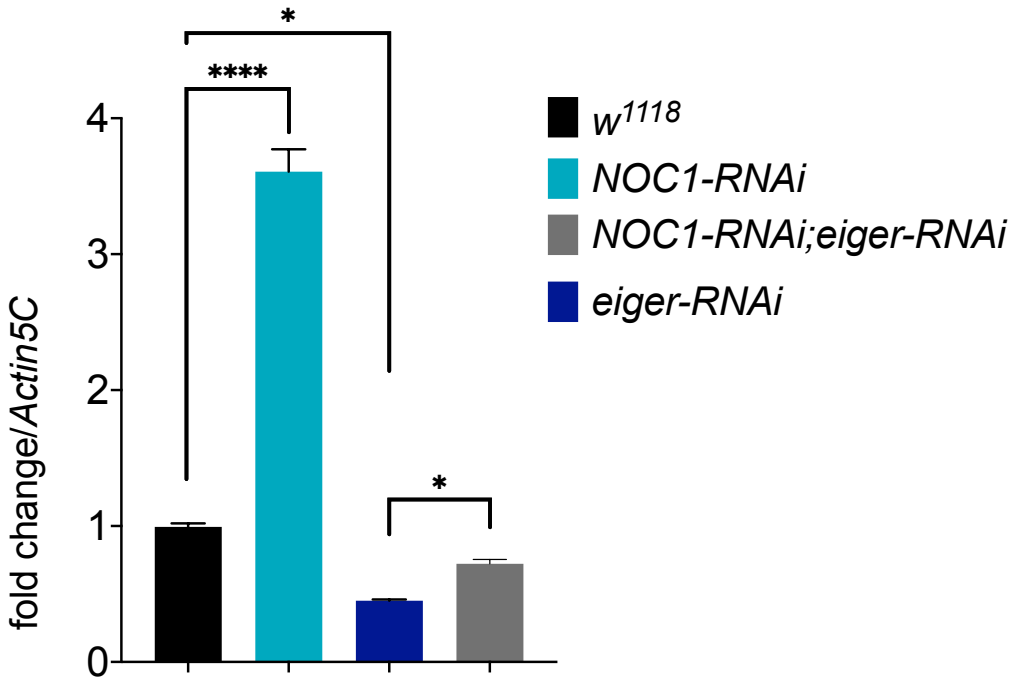

Fig. S7. qRT-PCR showing the relative amount of *eiger-mRNA* in wing imaginal discs from animals of the indicated genotypes. *NOC1-RNAi* or in combination with *eiger-RNAi* were expressed using the *nubbin-Gal4* promoter. RNA was extracted from imaginal discs. *p*-values were calculated with One-way ANOVA * = $p < 0.05$, **** = $p < 0.0001$, the error bars indicate the standard deviations.

Table S1. Selected list of potential targets of CEBPz involved in ribosomal biogenesis and nucleolar control. Data are from TCGA datasets from cBio Cancer Genomic Portal from Liver Hepatocellular Carcinoma (A) and Breast Cancer (B). *common proteins

A

liver tumor	p Value
DKC1/NOP60b	6.71E-15
FBL	0.000001171
NOP10	0.00007354
NOP16	0.000008451
NOP2*	1.59E-10
NOP56	0.000001243
NOP58	5.18E-14
RPS7*	5.54E-12
RPS16	0.0008972
RPS18	0.005751
RPS20	0.0000206
RPS21	0.0007177
RPS27A	1.23E-08
RPS2P32	0.0000032
RPSA	0.004546
RPL5	0.0005937
RPL7	0.0191
RPL21	0.0005989
RPL24*	0.00188
RPL30	0.00006775
RPL35A*	0.0001787
RPL38	0.0008094
RPL39	0.00004626

B

brast tumor	p Value
NOP2*	0.0454
RPS7*	3.36E-04
RPS8	0.0325
RPL5	0.0444
RPL12	0.0225
RPL14	0.0389
RPL24*	0.0333
RPL27	0.032
RPL32	0.047
RPL35	0.044
RPL35A*	0.0419

Table S2. List of PRIMERS used for qRT-PCRs

gene	5' FW sequence	5' REV sequence	reference
NOC1	CTATACGCTCCACCGCACAT	GTCGCTACCGAACTTGTCCA	this work
NOC2	AGGAGCTTGAAGGGCTTAAAGA	ATCCTTGCTGGGTTTGTGGTA	this work
NOC3	TGCAGGCAGGCAAAAATCAC	AGCAAGCGTTTCATGAAGGC	this work
E74b	GAATCCGTAGCCTCCGACTGT	AGGAGGGAGAGTGGTGGTGTT	(Colombani et al., 2005)
Actin5c	CAGATCATGTTCGAGACCTTCAAC	ACGACCGGAGGCGTACAG	(Colombani et al., 2005)
Dilp8	CGACAGAAG GTCCATCGAGT	GTT TTGCCG GATCCAAGTC	(Boulan et al., 2019)
NOC1 genomic	GTCACGGTCATTTCAATGGTA	CATGTCCAGCACCTCATC	this work
ITS1	GAAGAAACAAAATTCGAAAG	CGTATGCCCATAACTAAGAT	Neumuller et al., 2013)
ITS2	ATCTTAGTTATGGGCATACG	CTGGCATATATCAATTCCTT	(Neumuller et al., 201
18S	CTCATATCCGAGGCCCTGTA	ACGAACGTTTTAACCGCAAC	(Neumuller et al., 2013)
28S	CGCTACGTCCGTTGGATTAT	CAATGCAAATTGCCCCTTAT	(Neumuller et al., 2013)
XRP1	GACCACACCGGAGATTATCAA	GCTGGTACTGGTACTTGTGGTG	(Baillon et al., 2018)
Eiger	AAAGGTGGATGGCCTCACG	TGCCGGTATGTGCATTGTTG	this work

Baillon, L., Germani, F., Rockel, C., Hilchenbach, J. and Basler, K. (2018). Xrp1 is a transcription factor required for cell competition-driven elimination of loser cells. *Sci Rep* **8**, 17712.

Boulan, L., Andersen, D., Colombani, J., Boone, E. and Leopold, P. (2019). Inter-Organ Growth Coordination Is Mediated by the Xrp1-Dilp8 Axis in Drosophila. *Dev Cell* **49**, 811-818 e4.

Colombani, J., Bianchini, L., Layalle, S., Pondeville, E., Dauphin-Villemant, C., Antoniewski, C., Carre, C., Noselli, S. and Leopold, P. (2005). Antagonistic actions of ecdysone and insulins determine final size in Drosophila. *Science* **310**, 667-70.

Neumuller, R. A., Gross, T., Samsonova, A. A., Vinayagam, A., Buckner, M., Founk, K., Hu, Y., Sharifpoor, S., Rosebrock, A. P., Andrews, B. et al. (2013). Conserved regulators of nucleolar size revealed by global phenotypic analyses. *Sci Signal* **6**, ra70.

Port, F., Strein, C., Stricker, M., Rauscher, B., Heigwer, F., Zhou, J., Beyersdorffer, C., Frei, J., Hess, A., Kern, K. et al. (2020). A large-scale resource for tissue-specific CRISPR mutagenesis in Drosophila. *Elife* **9**.

Szklarczyk, D., Gable, A. L., Lyon, D., Junge, A., Wyder, S., Huerta-Cepas, J., Simonovic, M., Doncheva, N. T., Morris, J. H., Bork, P. et al. (2019). STRING v11: protein-protein association networks with increased coverage, supporting functional discovery in genome-wide experimental datasets. *Nucleic Acids Res* **47**, D607-D613.